Environmental Science & Technology

pubs.acs.org/est

Article

Isotopic Characterization of Mercury Atmosphere−Foliage and Atmosphere−Soil Exchange in a Swiss Subalpine Coniferous Forest

Chaoyue Chen, Jen-How Huang,* Kai Li, Stefan Osterwalder, Chenmeng Yang, Peter Waldner, Hui Zhang, Xuewu Fu, and Xinbin Feng*

Cite This: *Environ. Sci. Technol.* 2023, 57, 15892−15903

Read Online

ACCESS | Metrics & More | Article Recommendations | Supporting Information

ABSTRACT: To understand the role of vegetation and soil in regulating atmospheric Hg^0, exchange fluxes and isotope signatures of Hg were characterized using a dynamic flux bag/chamber at the atmosphere−foliage/soil interfaces at the Davos-Seehornwald forest, Switzerland. The foliage was a net Hg^0 sink and took up preferentially the light Hg isotopes, consequently resulting in large shifts (−3.27‰) in δ^{202}Hg values. The soil served mostly as net sources of atmospheric Hg^0 with higher Hg^0 emission from the moss-covered soils than from bare soils. The negative shift of δ^{202}Hg and Δ^{199}Hg values of the efflux air relative to ambient air and the $\Delta^{199}Hg/\Delta^{201}$Hg ratio among ambient air, efflux air, and soil pore gas highlight that Hg^0 re-emission was strongly constrained by soil pore gas evasion together with microbial reduction. The isotopic mass balance model indicates 8.4 times higher Hg^0 emission caused by pore gas evasion than surface soil photoreduction. Deposition of atmospheric Hg^0 to soil was noticeably 3.2 times higher than that to foliage, reflecting the high significance of the soil to influence atmospheric Hg^0 isotope signatures. This study improves our understanding of Hg atmosphere−foliage/soil exchange in subalpine coniferous forests, which is indispensable in the model assessment of forest Hg biogeochemical cycling.

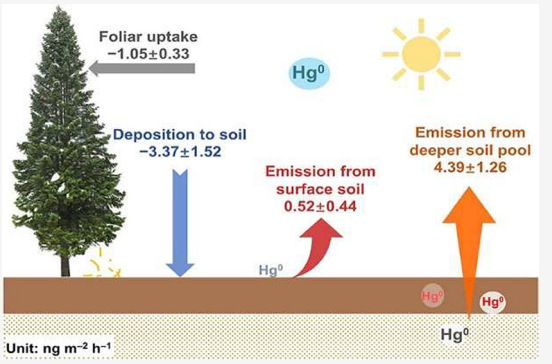

KEYWORDS: *atmospheric Hg^0, atmosphere−foliage/soil exchange, stable Hg isotopes, deposition, re-emission*

1. INTRODUCTION

Mercury (Hg) is a global pollutant of public concern due to its volatility, persistence, neurotoxic methylated species as well as bioconcentration and magnification effects.[1] Atmospheric Hg exists in three operationally defined forms: gaseous elemental mercury (Hg^0), gaseous oxidized Hg (GOM), and particulate-bound Hg (PBM). Hg^0 is usually the most abundant form in the troposphere because of its considerable chemical inertness, high volatility, and low deposition velocity.[2,3] It has a long residence time (0.5−2 years); thus, it is transported on a regional and global scale.[4,5] Ultimately, atmospheric Hg is deposited on the terrestrial environment and becomes a major source of Hg transported to adjacent freshwater aquatic ecosystems.[6,7]

Forest ecosystems account for 31% of global land areas and are hotspots for the global biogeochemical cycling of Hg.[8,9] A substantial quantity of anthropogenic Hg is accumulated and stored in forested ecosystems through (1) vegetation uptake, (2) precipitation, and (3) PBM and GOM deposition to forest surfaces. Among all, atmospheric Hg^0 sink via litterfall, wood, epiphyte, and throughfall accounts for 60−90% of total forested Hg input.[10,11] On the other hand, Hg outputs from forest ecosystems include (1) re-emissions of Hg that was previously deposited to vegetation and soils and (2) the forest floor surface runoff.[12] Recent studies have emphasized the crucial role of vegetation and the forest soil playing on Hg^0 dry deposition to terrestrial ecosystems, and this sink is estimated to be 1000−4000 Mg year^{-1}.[9,11,13−15] To date, atmosphere−surface Hg^0 exchange fluxes are still poorly constrained in the forest ecosystem,[16−18] which ranges between −727 and +703 Mg year^{-1}.[19] Major uncertainties as suggested by a recent study may stem from the few direct observations and the impact of environmental and ecological factors.[9]

It is generally acknowledged that terrestrial vegetation acts as a global Hg^0 pump, removing Hg from the atmosphere, mainly by foliar uptake. This process results in a seasonal pattern of observed atmospheric Hg^0 concentrations and isotope signatures.[13,14,20−22] However, direct observations of atmosphere−foliage Hg^0 exchange are rare but would be crucial to constrain the magnitude of Hg^0 fluxes in the many different forest ecosystems around the world.[19,23] Furthermore, it is unclear whether forest soils act as Hg^0 sinks or sources (i.e., Hg^0 deposition to soils directly; or Hg^0 re-emission from soils),

Received: May 11, 2023
Revised: August 17, 2023
Accepted: September 13, 2023
Published: October 3, 2023

which depend largely on the soil types and environmental conditions.[9,18,19] Recent studies have shown that atmosphere−soil Hg^0 exchange not only changes the concentrations but also affects the isotopic compositions of ambient Hg^0,[24,25] thus playing a key role in atmospheric Hg^0 cycling in the forest. Consequently, it is crucial to better elucidate atmosphere−vegetation and −soil Hg^0 exchange in forest ecosystems.

Today, long-term observations of Hg^0 concentration, Hg^0 exchange flux quantification with micrometeorological techniques at the ecosystem scale, and Hg^0 isotope measurements alone do not allow the identification and quantification of the magnitude of atmosphere−vegetation and atmosphere−soil Hg^0 exchange. This can be assessed by gas flux measurements using dynamic flux bags (DFBs) and dynamic flux chambers (DFCs) to investigate the relative contributions of foliage and soil on the net Hg balance in the ecosystem.[26] Mercury stable isotope analysis is an effective technique for determining sources and transformation mechanisms of Hg to study its biogeochemical cycling.[6] Generally, Hg isotopes may undergo both mass-dependent fractionation (MDF, reported as $\delta^{202}Hg$) as well as odd (odd-MIF, reported as $\Delta^{199}Hg$ and $\Delta^{201}Hg$) and even mass-independent fractionation (even-MIF, reported as $\Delta^{200}Hg$) in surface environments during a specific or multiple process of transport and transformation.[27] Different odd-MIF mechanisms and fractionation processes were known to yield different $\Delta^{199}Hg/\Delta^{201}Hg$ ratios. While the magnetic isotope effect (MIE) caused by photoreduction produced a $\Delta^{199}Hg/\Delta^{201}Hg$ ratio of ∼1,[28] dark reduction of Hg by organic matter due to nuclear volume effect (NVE) led to a $\Delta^{199}Hg/\Delta^{201}Hg$ ratio of ∼1.6.[29] To date, the Hg isotope composition of the sources and fractionation of many processes in forest ecosystems have already been well investigated.[30,31] Although Hg isotopic compositions of atmospheric Hg^0, foliage, and soil have been reported, information about the dynamic of Hg^0 flux components during foliar uptake and soil emission in boreal forests is rare.

Here, we employed enclosure methods, i.e., dynamic flux bag and chamber, to quantify atmosphere−foliage and atmosphere−soil Hg^0 exchange at the plot scale over one month period (October 2019) in a coniferous subalpine forest in Davos-Seehornwald, Switzerland. Our objectives were (1) to quantify near-ground atmosphere−foliage/soil Hg^0 exchange fluxes and to reveal the corresponding controlling factors, (2) to estimate the contribution of both vegetation (foliage and moss) uptake and soil re-emission processes to near-ground atmospheric Hg^0 concentration and isotope dynamics in the remote subalpine forest ecosystem, and (3) to highlight the potential sources and relevant mechanisms of Hg^0 re-emission from the forest soils.

2. MATERIALS AND METHODS

2.1. Site Description. The Davos-Seehornwald research site is located at 46.815°N, 9.856°E at 1639 m a.s.l. in the middle range of the subalpine belt in the eastern part of the Swiss Alps. The research site is an Integrated Carbon Observation System (ICOS) Class 1 ecosystem station since November 2019 (https://www.icos-switzerland.ch/davos). The average annual precipitation is 1020 mm, and the average annual temperature in this region is 4.5 °C (2009−2020), increased by +0.4 °C compared to 1997−2008 (https://www.swissfluxnet.ethz.ch). The coniferous forest is dominated by Norway spruce (*Picea abies* (L.) Karst.) with an average canopy height of 18 m, and a leaf area index of about 3.9 m^2 m^{-2}. The tree age averages about 100 years, with some trees reaching 300 years. The understory vegetation is rather patchy, covering roughly 30% of the forest floor, and is mainly composed of dwarf shrubs and mosses. The soil type is Chromic Cambisols and Rustic Podsols with pH of 3.5−5.5 and a forest floor thickness of 5−10 cm.[32,33]

2.2. Measurement of the Atmosphere−Foliage Hg^0 Exchange Flux. Atmosphere−foliage Hg^0 exchange flux measurements at the branch level were performed for 14 days (October 17−30, 2019) on spruce trees in Davos-Seehornwald. The Tedlar dynamic flux bag (DFB) method used here has been applied to atmosphere−foliage Hg^0 exchange measurements previously.[34,35] The DFB is custom-made with heat-sealed polyvinyl fluoride film (Tedlar, 51 μm thickness), with a maximum volume of 80 L and three flow valve switches distributed on both sides of it. One switch was connected to a Teflon channel pump (KNF Neuberger, Germany) using a 1/2 inch Teflon tube to pump ambient air into DFB at 10 L min^{-1}. Another switch was connected to the pump using a 1/2 inch Teflon tube to extract air from DFB. The DFB inlet and outlet were connected to a synchronized multiport sampling system (Model 1115, Tekran Instruments, Corp., Canada) using 1/4 inch Teflon tubes and then combined with an automated ambient air analyzer (Model 2537X, Tekran Instruments, Corp., Canada) for Hg^0 concentration measurement. A sketch of the setup is shown in Figure S9. The inlet and outlet air were sampled at 7 L min^{-1} into chlorine-impregnated activated carbon (ClC) traps for stable Hg^0 isotope measurement. Finally, the atmosphere−foliage Hg^0 exchange flux was calculated as follows:

$$F = \frac{Q}{S} \cdot (C_{out} - C_{in}) \quad (1)$$

where C_{out} and C_{in} are the Hg^0 concentrations of the outlet and inlet air of DFB (ng m^{-3}), respectively; Q is the DFB internal flushing flow rate of air (m^3 h^{-1}); S is the total enclosed leaf surface area (m^{-2}); and F is the foliage Hg^0 flux. A positive value of F indicates net Hg^0 release from foliage to the atmosphere and a negative F represents net Hg^0 uptake by foliage. Meteorological data such as solar radiation (SR), relative humidity (RH), and air temperature (AT) were obtained from the research site.

2.3. Measurement of the Atmosphere−Soil Hg^0 Exchange Flux. Atmosphere−soil Hg^0 exchange flux measurements were performed for 14 days (October 10−23, 2019) below the canopy in Davos-Seehornwald. The surface soil of the Davos-Seehornwald forest is mainly composed of organic and mineral soil materials as well as moss patches (48%) of various sizes. Two subplots of moss-covered soil and two subplots of bare soil were randomly selected to carry out atmosphere−soil surface Hg^0 exchange measurements. Each flux measurement lasted over a 3−5-day period using the dynamic flux chamber (DFC) method described in the earlier work.[36−38] The DFC is a rectangular parallelepiped with a bottom opening of 30 cm × 30 cm. The covered soil surface area of DFC is 0.09 m^2, and the air inlet channel had 20 small holes with a diameter of 1 cm. Local fine-grained soil was placed outside the chamber to seal any gaps between the bottom of the chamber and the soil. The DFC inlet and outlet were connected to the synchronized multiport sampling system (Model 1115, Tekran Instruments, Corp., Canada), and a Teflon tube with 1/4 inch outside diameter was connected to a Tekran 2537X to measure Hg^0 concentration of ambient air

https://doi.org/10.1021/acs.est.3c03576
Environ. Sci. Technol. 2023, 57, 15892−15903

and efflux air, respectively. The Hg^0 flux was calculated by the equation as follows:

$$F = \frac{Q}{A} \cdot (C_i - C_0) \quad (2)$$

where F is soil Hg^0 flux (ng m^{-2} h^{-1}), Q is the DFC internal flushing flow rate of air (m^3 h^{-1}), A is the area enclosed by the chamber (m^2), and C_i and C_0 are the Hg^0 concentration of the DFC outlet and inlet air, respectively (ng m^{-3}). A positive value of F indicates Hg^0 release from the soil to the atmosphere, and a negative value of F indicates Hg^0 deposition to the soil. Meteorological data such as solar radiation (SR), soil water content (WC), soil temperature (ST), and air temperature (AT) were obtained from observations at the Davos-Seehornwald station.

2.4. Sampling, Preconcentration, and Hg Concentration Analysis. The self-made cake-shaped Teflon hollow disc (diameter 200 mm, thickness 30 mm) was used to sample soil pore gas for Hg isotope measurement. The entire disc was evenly distributed with small holes with a diameter of 2 mm, and a 1/4 inch Teflon tube was connected to the position of the disc core. Two identical discs were placed in a soil layer of 5−10 cm at a distance of 2 m. Two Teflon tubes are connected by a Teflon tee and introduced into a CLC trap, followed by a KNF pump and a flow meter. The flow rate of the pump was 0.5 L min^{-1}. The pump was opened by the control system at 8:00/16:00/24:00 every day to extract for 1 h. Each soil pore gas sampling lasted for 2−3 months.

Traps containing 0.7 g of ClC material were utilized to collect both Hg^0 in the inlet air and the outlet air of DFB as well as DFC for isotope analysis using a pump (KNF Neuberger, Germany). We obtained two flux samples exposed to the air with a sampling period of 2−4 days. The foliage enclosed in DFB and surface soil covered by DFC at 0−10 cm depth were sampled at the end of each observation. The leaf area of the foliage was determined using a calibrated computer scanner and ImageJ software (NIH, U.S.A.). The collected foliage samples were oven-dried at 65 °C until a mass variation of less than 0.03% in 8 h and soil samples were freeze-dried, then ground, homogenized, and stored in sealed plastic bags before analysis. Total Hg concentrations in foliage and soil samples were measured with a DMA-80 direct Hg analyzer (Milestone, Italy). The National Institute of Metrology (NIM, China) solid standard reference materials GBW07405 (GSS-5, Yellow-red Soil: Hg: 290 ± 40 ng g^{-1}) and GBW10020 (GSB-11, Quince Leaves: Hg: 150 ± 25 ng g^{-1}) were taken as soil and vegetation Hg standards, yielding recoveries of 106 ± 9% (n = 3) and 89 ± 8% (n = 4), respectively.

Foliage, soils, and the exposed ClC-trap samples were processed with a double-stage offline combustion-trapping technique.[39] Mercury in the samples was completely vaporized in a tube furnace and finally trapped with a 5 mL oxidizing solution of 40% mixture of 16 M HNO_3 and 12 M HCl (2:1, v/v).[40] Mercury concentrations in the oxidizing solution were analyzed using a cold vapor atomic fluorescence spectrometry (Model 2500, Tekran Instruments, Corp., Canada) following the US-EPA method 1631.[41] A mean preconcentration recovery of combustion of lichen certified reference material (BCR 482, 480 ± 20 ng Hg g^{-1}) using the double-stage offline combustion-trapping technique was determined to be 89 ± 6% (1SD, n = 3).

2.5. Hg Isotope Measurements. Mercury isotope compositions were measured by a multicollector inductively coupled plasma mass spectrometer (MC-ICP-MS, Neptune II, Thermo Scientific, USA) using the cold vapor phase separator system as the introduction system (Figure S8), following the study of Yin et al.[42] Before Hg isotope measurements, trap solutions were diluted to a concentration of ∼1 ng Hg mL^{-1} with ultrapure water. The diluted trap solutions or Hg standard coupled with the reducing agent (3% $SnCl_2$) were introduced inline to a continuous flow cold vapor phase separator system to generate Hg vapor. Tl aerosol (NIST SRM 997) generated by an Apex-Q desolvation unit (Elemental Scientific Inc., USA) was used for instrumental mass bias correction. Finally, the reduced Hg vapor mixed with a Tl aerosol was carried by argon carrier gas to MC-ICP-MS. The measurement process followed the standard-sample-standard protocol by using the standard NIST SRM 3133. All samples or Hg standards were analyzed in one block with 50 cycles to improve the internal precision. Following Blum and Bergquist,[43] MDF is reported in the "δ" notation as follows:

$$\delta^{202}\mathrm{Hg}(‰) = \left[\frac{\left(\frac{^{202}\mathrm{Hg}}{^{198}\mathrm{Hg}}\right)_{\mathrm{sample}}}{\left(\frac{^{202}\mathrm{Hg}}{^{198}\mathrm{Hg}}\right)_{\mathrm{NIST3133}}} - 1 \right] \times 1000 \quad (3)$$

MIF values are reported by using "Δ" notation and calculated by the following equation:

$$\Delta^{199}\mathrm{Hg}(‰) = \delta^{199}\mathrm{Hg} - (0.2520 \times \delta^{202}\mathrm{Hg}) \quad (4)$$

$$\Delta^{200}\mathrm{Hg}(‰) = \delta^{200}\mathrm{Hg} - (0.5024 \times \delta^{202}\mathrm{Hg}) \quad (5)$$

$$\Delta^{201}\mathrm{Hg}(‰) = \delta^{201}\mathrm{Hg} - (0.7520 \times \delta^{202}\mathrm{Hg}) \quad (6)$$

The NIST SRM 3177 secondary standard was analyzed for every 10 samples. Analytical uncertainties on measured isotope ratios were assessed by repeated analysis of the isotopic compositions of NIST SRM 3177 and CRM (BCR-482). Results of NIST SRM 3177 (δ^{202}Hg = −0.52 ± 0.09‰, Δ^{199}Hg = −0.01 ± 0.08‰, Δ^{200}Hg = 0.02 ± 0.10‰, Δ^{201}Hg = −0.02 ± 0.09‰, 2SD, n = 12) and BCR-482 (δ^{202}Hg = −1.61 ± 0.09‰, Δ^{199}Hg = −0.65 ± 0.02‰, Δ^{200}Hg = 0.08 ± 0.06‰, Δ^{201}Hg = −0.64 ± 0.09‰, 2SD, n = 7) were consistent with previously reported values.[20,34,44]

2.6. Quality Assurance and Quality Control. To ensure the accuracy of Hg^0 concentration measurements, the continuous monitoring system was regularly maintained and calibrated during observations. The particulate filter membrane on the air inlet was replaced every 5 days. In addition, the soda-lime tank after the intake air and the filter membrane before the Hg analyzer were replaced weekly. The internal Hg source of Tekran 2537X performed an automatic calibration every 25 h, and the two manual calibrations were performed using the external Hg source (Model 2505, Tekran Instruments, Corp., Canada) at the beginning and the end.

Prior to each experiment, blank tests were performed for DFB and DFC. The DFB was tightly sealed with nylon tape, and the bottom of the DFC was sealed with a Teflon membrane to compare Hg^0 concentration and isotope composition between inlet and outlet air. The Hg^0 concentrations of outlet air have no systematic difference with inlet air for DFB (0.017 ± 0.020, t test, n = 139, p = 0.73) and DFC (0.008 ± 0.035, t test, n = 62, p = 0.68) during the blank test period, respectively. The Hg^0 isotope compositions of outlet air were similar to those of inlet air for DFB and DFC

https://doi.org/10.1021/acs.est.3c03576
Environ. Sci. Technol. 2023, 57, 15892−15903

Table 1. Ambient Air Hg^0 Concentrations (ng m^{-3}) and Hg^0 Atmosphere−Foliage and Atmosphere−Soil Exchange Fluxes (ng m^{-2} h^{-1}) of Davos-Seehornwald in Switzerland Measured in October 2019

	atmosphere−foliage			atmosphere−bare soil		atmosphere−soil with moss	
	ambient air Hg^0	flux (per area of leaves)	flux (per area of ground)	ambient air Hg^0	flux	ambient air Hg^0	flux
average	0.86	−0.27	−1.05	0.84	1.17	0.83	1.93
Sd	0.11	0.08	0.33	0.13	1.06	0.10	1.13
median	0.87	−0.27	−1.05	0.82	0.99	0.83	1.74
min	0.21	−0.49	−1.90	0.39	−0.55	0.59	0.01
max	1.20	0.59	2.28	1.13	6.22	1.08	5.86

(Table S1). Consequently, the bag and chamber blanks do not affect atmosphere−surface Hg^0 exchange determination and isotope variations. Before air samples were collected in the field, a series of tests with ClC-traps including blank and breakthrough tests were conducted in the laboratory. The mean blank of 0.7 g of ClC materials was 91.2 ± 10.6 pg (1SD, n = 3), which was less than 1% of Hg in the collected air samples (13.6 ± 3.7 ng, 1SD, n = 30). Breakthrough tests showed that 98.1 ± 0.1% (1SD, n = 4) of Hg^0 in ambient air could be collected by the ClC traps at a similar flow rate to sampling. The recovery rate for all ClC-trap samples in field samples was 101.5 ± 10.1% (1SD, n = 28) (Table S4). Considering the synergistic effects from multiple factors, the structural equation model (SEM) was performed to quantitatively describe the driving factors affecting the atmosphere−foliage and −soil Hg^0 exchange flux using Amos 24.0 software.

3. RESULTS AND DISCUSSION

3.1. Atmosphere−Foliage Hg^0 Exchange. The net atmosphere−foliage Hg^0 exchange flux was steadily negative with a median value of −0.27 ng m^{-2} h^{-1} (per area of leaves) during the period of investigation, reflecting Norway spruce needles in Davos-Seehornwald as a sink of atmospheric Hg^0 (Table 1 and Figure S1). Similar foliar Hg uptake rates were observed from coniferous trees at the Hölstein research site in Switzerland (−0.29 ± 0.11 ng m^{-2} h^{-1}).[45] In comparison, at least doubled Hg^0 deposition rates from the atmosphere to foliage were found in deciduous forests in North America (−0.55 ± 0.06 ng m^{-2} h^{-1}), Central Europe (−0.84 ± 0.11 ng m^{-2} h^{-1}), Northern China (−1.2 ± 0.6 ng m^{-2} h^{-1}), and Southern China (−0.98 ± 0.27 ng m^{-2} h^{-1}).[14,34,35,45] Lower Hg^0 uptake rates by needles were mainly due to the relatively low stomatal conductance compared to broad leaves.[46,47] Relatively lower atmospheric Hg^0 concentrations (0.86 ± 0.11 ng m^{-3}) can also result in low needle uptake rates in Davos-Seehornwald than those at the aforementioned sites (Table 1). Also, plants grow usually slower in colder and drier boreal forests than in subtropical evergreen forests, leading to lower foliar Hg^0 uptake rates.[34,48]

Atmosphere−foliage Hg^0 exchange may be influenced by atmospheric Hg^0 concentrations, physiological parameters (e.g., net photosynthesis, tissue age, and specific leaf area), and meteorological conditions such as air temperature, humidity, and solar radiation.[49−51] In Davos-Seehornwald, the lack of a significant correlation between flux and ambient air Hg^0 concentrations revealed little effect of Hg^0 concentration on Hg uptake by Norway spruce in the background area (Figure S3). The SEM results show that the observed Hg^0 atmosphere−foliage exchange fluxes had no obvious correlation with meteorological parameters, which was inconsistent with previous studies (Figure S4a).[34,52] This reflects that the uptake of atmospheric Hg^0 by spruce was mainly controlled by physiological characteristics of the needle such as stomatal conductance, while meteorological factors had limited influence. The stomata difference among different vegetation species has been demonstrated to influence the uptake rates of atmospheric Hg^0.[46,48] While stomatal uptake is likely the main pathway of Hg accumulation in leaves,[46,53] more research is needed to pinpoint the physiological factors controlling the uptake rate of atmospheric Hg^0 by different plant species.

3.2. Hg Isotopic Compositions in Foliage, Ambient, and Efflux Air. As illustrated in Figure 1 and listed in Table S4, the isotopic compositions of atmospheric Hg^0 from Davos-Seehornwald forest characterized positive $\delta^{202}Hg$, negative $\Delta^{199}Hg$, and slightly negative $\Delta^{200}Hg$ ($\delta^{202}Hg$: 0.72 ± 0.38‰, $\Delta^{199}Hg$: −0.24 ± 0.03‰, $\Delta^{200}Hg$: −0.09 ± 0.05‰, 1SD, n = 5), matching background fingerprints from remote forest sites worldwide.[20,44,54,55] The foliages in the Davos-Seehornwald forest exhibited small ranges, with values of −2.54 ± 0.15‰ (1SD, n = 4) for $\delta^{202}Hg$ and −0.23 ± 0.05‰ (1SD, n = 4) for $\Delta^{199}Hg$ (Table S3). In the case of $\delta^{202}Hg$, the Davos-Seehornwald foliage had similar values to those of European and US foliage ($\delta^{202}Hg$: −2.24 ± 0.26‰, 1SD, n = 32) but significantly more positive values than those of Chinese foliages ($\delta^{202}Hg$: −3.00 ± 0.39‰, 1SD, n = 39, t test, p < 0.01) (Figure 1).[34,56−58] In comparison, the difference in $\Delta^{199}Hg$ between the foliage Hg in Seehornwald and

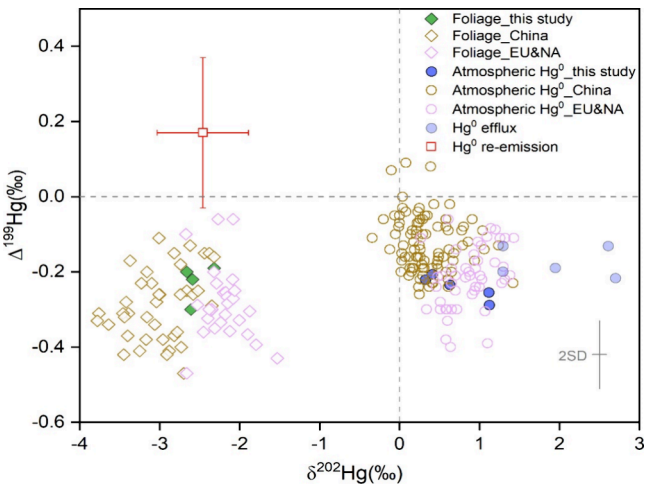

Figure 1. Mercury (Hg) isotopic compositions of the foliage and atmospheric Hg^0 during atmosphere−foliage exchange determined in October 2019 in Davos-Seehornwald, Switzerland, in comparison with those from Chinese, European, and North American forests.[14,20,34,44,54−58,60,90] The error bars represent ±2 standard deviation. Hg^0 re-emission isotopic composition data from Yuan et al.[34] are shown as the mean value with ±1 standard deviation.

https://doi.org/10.1021/acs.est.3c03576
Environ. Sci. Technol. 2023, 57, 15892−15903

atmospheric Hg^0 was insignificant. Nevertheless, the values of the Seehornwald foliage $\Delta^{199}Hg$ and $\Delta^{200}Hg$ were significantly lower than those of atmospheric Hg^{II} (precipitation, reactive Hg) reported worldwide (t test, $p < 0.01$) ($\Delta^{199}Hg$: −0.01 to 1.16‰, $\Delta^{200}Hg$: 0.08 to 1.18‰, n = 58).[44,59−61] These altogether suggest that Hg in foliage is mainly originated from atmospheric Hg^0. Leaf $\delta^{202}Hg$ values were significantly lower than the atmospheric ones (t test, $p < 0.01$), indicating that the needles tended to enrich light isotopes from the atmosphere. Vegetation uptake of Hg has been known to cause a negative $\delta^{202}Hg$ shift (−4.0 to −1.0‰) but a negligible $\Delta^{199}Hg$ shift between foliage and atmospheric Hg^0.[21,44,54] Our observation of a −3.27‰ shift in $\delta^{202}Hg$ between foliage and Hg^0 was therefore consistent with previous findings.[34,54]

We compiled literature on foliage and atmospheric Hg^0 isotope data from different remote forests (China, Europe, and North America) (Figure 1). Comparing the isotopic compositions of atmospheric Hg^0 from European and North American forests ($\delta^{202}Hg$: 0.87 ± 0.30‰, $\Delta^{199}Hg$: −0.22 ± 0.08‰, 1SD, n = 48), more negative $\delta^{202}Hg$ and more positive $\Delta^{199}Hg$ values ($\delta^{202}Hg$: 0.34 ± 0.31‰, $\Delta^{199}Hg$: −0.12 ± 0.07‰, 1SD, n = 92) were observed in Hg^0 from China (t test, all $p < 0.01$). As atmospheric Hg^0 of anthropogenic origins has usually a negative $\delta^{202}Hg$ and near-zero $\Delta^{199}Hg$ values,[59] the forest ecosystems in China are more strongly influenced by human activities than those in Europe and North America.[62] The higher anthropogenic Hg emissions from China (∼9000 Mg) compared to Europe (∼1760 Mg) and North America (∼2350 Mg) over the past two decades were also reflected in the atmospheric Hg^0 concentrations in forested ecosystems.[14,20,44,54,63−65] On the other hand, vegetation uptake, vegetation and soil re-emission, and atmospheric transformations of Hg may also contribute to differences in regional atmospheric Hg^0 isotopic signatures.[34,54,66] For instance, our experimental results show that the efflux Hg^0 (1.97 ± 0.68‰, 1SD, n = 5) had much higher $\delta^{202}Hg$ values than ambient air (0.72 ± 0.38‰, 1SD, n = 5) (Figure 1 and Table S4). Such an effect could be anticipated as the lower foliage $\delta^{202}Hg$ values, leading to higher $\delta^{202}Hg$ values of residual Hg^0. Therefore, foliar uptake of Hg^0 can result in a positive shift of $\delta^{202}Hg$ values of atmospheric Hg^0. That is why previous studies have reported higher atmospheric $\delta^{202}Hg^0$ values in vegetation-covered than bare areas.[55,67] The effect of soil Hg emission on local atmospheric Hg^0 isotopic compositions will be discussed in Section 3.4.

Compared to Europe and North America ($\delta^{202}Hg$: −2.24 ± 0.26‰, 1SD, n = 32), the Chinese foliage has significantly more negative $\delta^{202}Hg$ values ($\delta^{202}Hg$: −3.00 ± 0.39‰, 1SD, n = 39) (t test, $p < 0.01$). Mercury isotopic compositions of foliage can be affected by sources, species, physiological properties, climate, and re-emission process.[34,58] As a whole, the shift in $\delta^{202}Hg$ from the corresponding atmospheric Hg^0 to Hg in vegetation leaves were similar in Davos-Seehornwald (−3.27‰), in China (−3.34‰) as well as Europe and North American (−3.11‰) (Figure 1). Such a comparison reveals that vegetation, physiological characteristics, and climate differences cannot fully explain the deviation of $\delta^{202}Hg$ in foliage among Chinese, European and North American vegetation ($\delta^{202}Hg_{China-EU\&NA}$ = −0.76‰). Since Hg^0 re-emission from vegetation has a similar $\delta^{202}Hg$ value to that of leaves,[34] the re-emission process could not significantly change $\delta^{202}Hg$ value of leaves. Thus, the more negative $\delta^{202}Hg$ of leaves in Chinese forests are mainly due to the local atmospheric Hg^0 with more negative $\delta^{202}Hg$.[62]

3.3. Atmosphere−Soil Hg^0 Exchange. The arithmetic mean values of the atmosphere−soil Hg^0 flux in the study period were 1.93 ± 1.13 ng m^{-2} h^{-1} (range: 0.01−5.86 ng m^{-2} h^{-1}) and 1.17 ± 1.06 ng m^{-2} h^{-1} (−0.55 to 6.22 ng m^{-2} h^{-1}) for the moss-covered and bare subplots, respectively (Table 1, Figure S2), consistent well with the recent observation in a NE-Chinese temperate forest (1.10−6.0 ng m^{-2} h^{-1}).[14] In comparison, atmosphere−soil Hg^0 fluxes in Davos-Seehornwald were remarkably higher than those earlier determined in other temperate/boreal forests in Europe (Table S2), but much lower than those measured in subtropical forests in S-China, such as Mt. Ailao (−3.87 to 11.75 ng m^{-2} h^{-1}) and Mt. Gongga (−6.20 to 21.10 ng m^{-2} h^{-1}).[37,68] The soil Hg concentrations influenced the atmosphere−soil Hg^0 fluxes little here since the soils at the aforementioned sites were all background forest soils.

We observed clear diurnal patterns of the atmosphere−soil Hg^0 exchange fluxes, light intensity, and air temperature (Figure S2). The Hg^0 exchange was clearly elevated during 08:00−17:00. Ambient air Hg^0 concentrations were slightly elevated during the daytime. Almost all atmosphere−soil Hg^0 exchange measurements were positive, including in moss-covered areas, indicating the surface soil as a net source of Hg^0. The only few exceptions with negative atmosphere−soil Hg^0 exchange (−0.13 ± 0.49 ng m^{-2} h^{-1}) were measured in the early morning at about 5:00, reflecting net Hg^0 deposition to soils when the air temperature was low (Figure S2a).[69,70] On the basis of SEM analysis, the air temperature (normalized path coefficient: 0.54−0.67) was the main driver governing atmosphere−soil Hg^0 exchange (Figure S4b,c), which was consistent with the effect of temperature on atmosphere−soil Hg^0 exchange flux diurnal patterns. The regression equations of the Hg^0 flux versus the inverse of the temperature follow the Arrhenius equation (Figure S5). Previous studies also have shown that temperature is one of the main factors determining the atmosphere−soil Hg^0 flux in forest ecosystems.[37,71,72]

It is worth noting that the average flux of Hg^0 emission from the moss-covered soil was nearly twice that from the bare soil (Table 1), which reveals the important role of moss in influencing soil Hg^0 re-emission. Several studies have suggested that Hg^0 release from vegetation was mainly caused by photoreduction.[34,73,74] However, the emission fluxes from moss-covered soils were higher than bare soils occurring not only during the daytime (08:00−17:00, t test, $p < 0.05$) but also at night (17:00−08:00, t test, $p < 0.05$) (Figure S2). This indicates that processes other than photoreduction drove the elevated Hg^0 emission from moss-covered soils. Such processes likely include changes in the physicochemical or biological properties of the moss-underlying soil. Similarly, many studies have found that CO_2 emissions from bare soils were lower than from the moss-dominated forest floor.[75,76] In comparison, different Hg^0 re-emission rates caused by the changes in the soil physicochemical properties could be generally excluded. We found no significant differences in soil Hg content, soil temperature, and soil water content between moss-covered and bare soils in Seehornwald (Figure S6 and Table S3), which may influence the Hg^0 emission rate in soils.[37,77] Soil pH was demonstrated to correlate positively with soil Hg re-emission.[78] Nevertheless, our moss-covered soils (3.4−3.5) had lower pH than bare soils (3.9−4.2) but higher soil Hg re-emission (Tables 1 and S3), reflecting soil pH played a minor

https://doi.org/10.1021/acs.est.3c03576
Environ. Sci. Technol. 2023, 57, 15892−15903

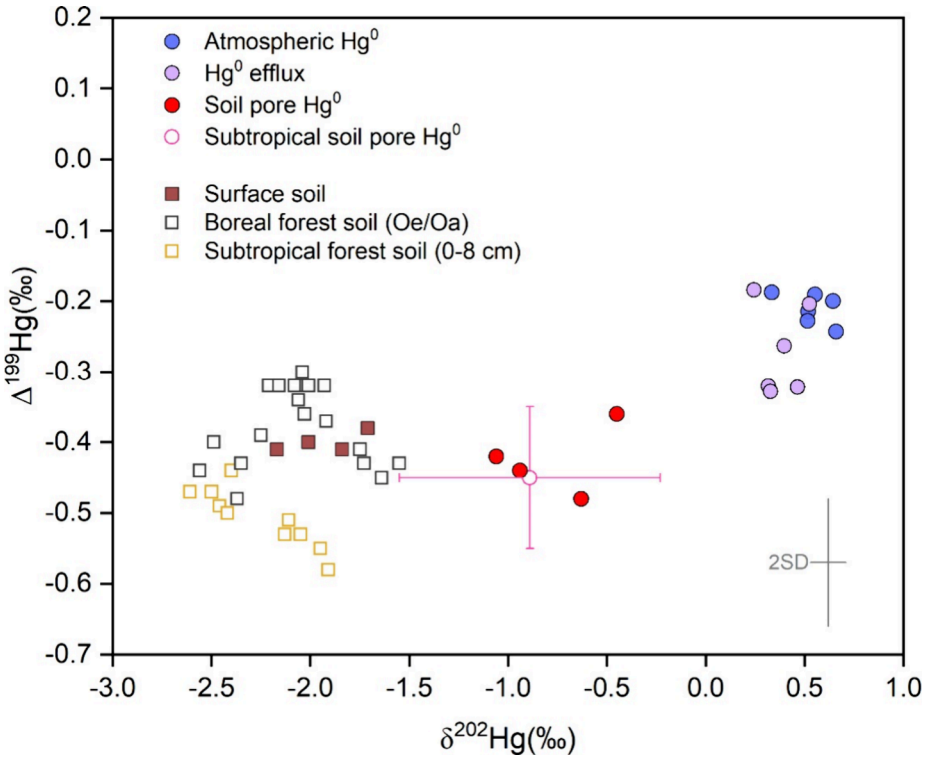

Figure 2. Mercury isotopic compositions of atmospheric Hg^0, efflux air Hg^0, and surface soil during atmosphere−soil exchange determined in October 2019 as well as soil pore Hg^0 sampled in different seasons in 2019 in Davos-Seehornwald, Switzerland. The error bars represent ±2 standard deviation. The surface soils of boreal and subtropical forest isotopic data were from Jiskra et al.[82] and Yuan et al.,[24] respectively. Subtropical soil pore gas Hg^0 isotopic composition data from Yuan et al.[24] are shown as the mean value with ±1 standard deviation.

role here. In concert with our findings, Sun et al.[76] found no difference in soil temperature and soil water content but higher microbial activity in moss-covered than bare soils of a subalpine forest on the east edge of the Tibet Plateau. The increased microbial activity could result in about 85% higher CO_2 emissions.[76] Microbial reduction is one of the most important processes responsible for soil Hg reduction to Hg^0.[79−81] We suggest that the higher Hg^0 emission from moss-covered soils compared to bare soils was related to higher biotic Hg reduction rates, which was also supported by the Hg isotopic characteristics and results from the isotopic mass balance model (see details below).

3.4. Hg Isotopic Compositions in Soil, Soil Pore Gas, and Flux Components. The surface soil in Davos-Seehornwald exhibited negative δ^{202}Hg (−1.93 ± 0.20‰, 1SD, n = 4), Δ^{199}Hg (−0.40 ± 0.01‰, 1SD, n = 4), and insignificant Δ^{200}Hg (0.00 ± 0.03‰, 1SD, n = 4) (Figure 2 and Table S3), agreeing with the finding in the Swedish boreal forest.[82] The more positive MDF and odd-MIF in our soils than in the subtropical forest soil in China were more likely derived from different Hg sources and fractionations during postdepositional process.[81] Compared to the isotopic compositions of the surface soil, more positive δ^{202}Hg values ($\delta^{202}Hg_{pore\ gas-soil}$ = 1.16‰) were observed in soil pore Hg^0 (δ^{202}Hg: −0.77 ± 0.28‰, 1SD, n = 4) (t test, p < 0.01). Such positive δ^{202}Hg shift between soil pore Hg^0 and soil was similar to that in the subtropical forest (1−2‰) but with a different magnitude.[24] Namely, emission of Hg^0 to near-ground air could lead to heavier δ^{202}Hg of soil pore gas, which was strongly affected by Hg^0 concentration gradient, pore space, soil water content and soil type.[24] Similar to the subtropical forest, Δ^{199}Hg signature of the soil pore gas (Δ^{199}Hg = −0.43 ± 0.05‰, 1SD, n = 4) was comparable to the corresponding surface soil (Δ^{199}Hg = −0.40 ± 0.01‰, 1SD, n = 4) in Davos-Seehornwald. Based on the two comparisons above, the formation process of the soil pore Hg^0 pool in temperate and subtropical forests could be very similar. Usually, microbial Hg reduction does not cause odd-MIF, whereas abiotic dark reduction mediated by organic matter produces a small positive odd-MIF shift in the product Hg^0.[29,80] Moreover, the concentration of soil pore Hg^0 was much higher than that of the near-ground air (Tables S4 and S5). These altogether reflect the soil pore Hg^0 pool in Davos-Seehornwald forest soil arising predominately from microbial and dark reduction.

During the period of investigation, small but significant difference of δ^{202}Hg were detected (paired sample t test, p < 0.01) between ambient air Hg^0 (δ^{202}Hg = 0.54 ± 0.12‰, Δ^{199}Hg = −0.21 ± 0.02‰, 1SD, n = 6) and soil efflux air Hg^0 (δ^{202}Hg = 0.38 ± 0.10‰, Δ^{199}Hg = −0.27 ± 0.07‰, 1SD, n = 6) through DFC (Figure 2 and Table S4). A recent study suggested that atmospheric Hg^0 deposition into soils followed kinetic isotope fractionation with an MDF enrichment factor of −4.32 ± 0.83‰ and a negligible odd-MIF.[25] Therefore, the absorption of atmospheric Hg^0 by the soil will not lead to any negative shifts of MDF and odd-MIF. The re-emitted Hg^0 to the near-surface atmosphere is derived from (1) Hg photoreduction in the uppermost layer of the forest soil and (2) diffusion from porous organic horizons driven by the Hg^0 concentration gradient between the near-surface air and soil pore gas.[24,25,83] Photoreduction process may be restricted due to the limited solar radiation that actually penetrates the dense canopy of the subalpine coniferous forest,[19] which is verified in this study by about 90% decrease in solar radiation under the canopy and the trivial effect of solar radiation on Hg^0 exchange

https://doi.org/10.1021/acs.est.3c03576
Environ. Sci. Technol. 2023, 57, 15892−15903

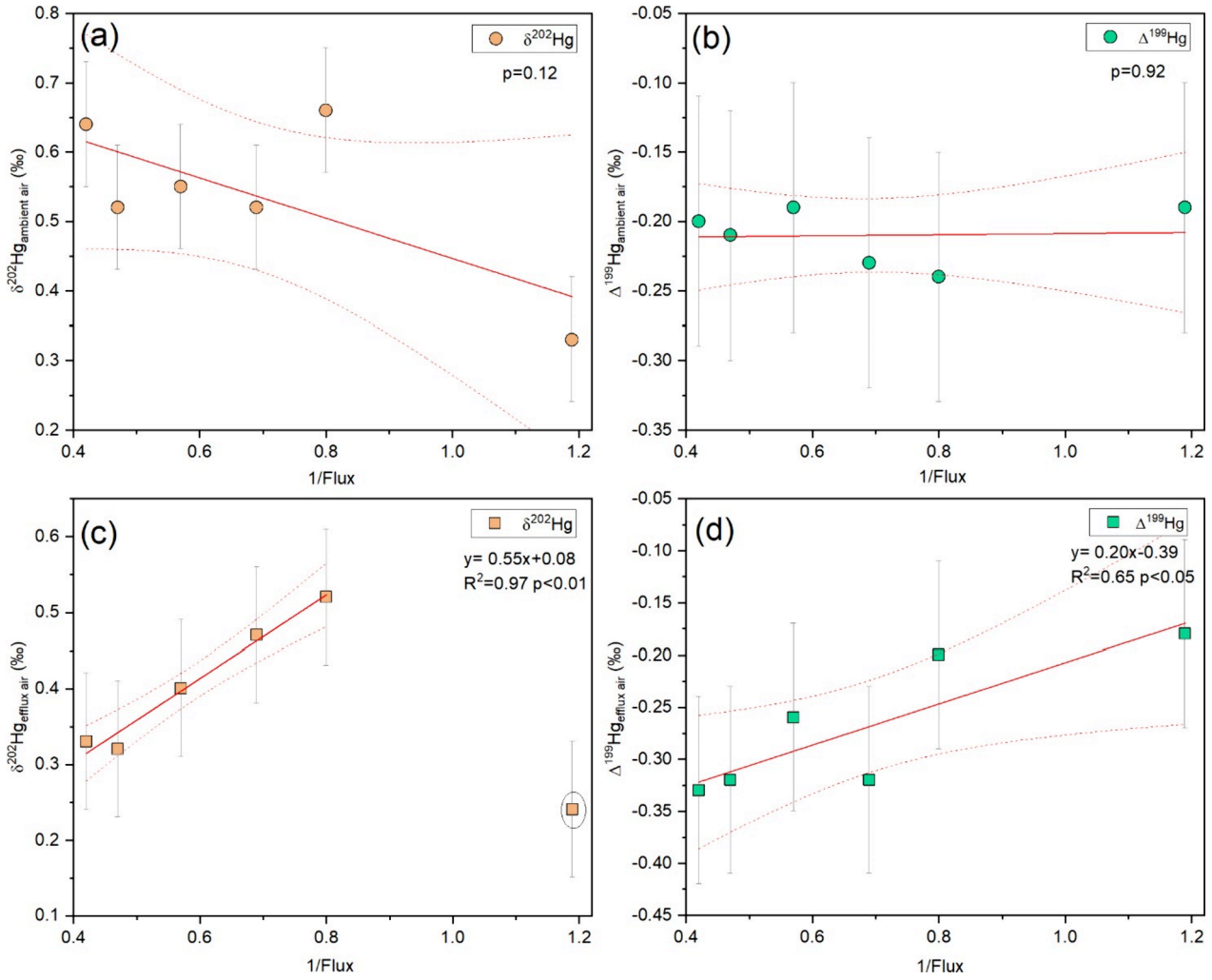

Figure 3. Scatterplot of Hg isotopic signatures vs Hg^0 1/flux on the basis of all atmosphere-soil exchange measurements performed in Davos-Seehornwald, Switzerland. (a) δ^{202}Hg vs 1/flux, (b) Δ^{199}Hg vs 1/flux in the ambient air. (c) δ^{202}Hg vs 1/flux and (d) Δ^{199}Hg vs 1/flux in the efflux air. The red straight lines represent the regression fitting results, and the red envelopes represent the 95% confidence interval. The encircled point is not included in the present fit line in (c). The error bars represent ±2 standard deviation for Hg isotope.

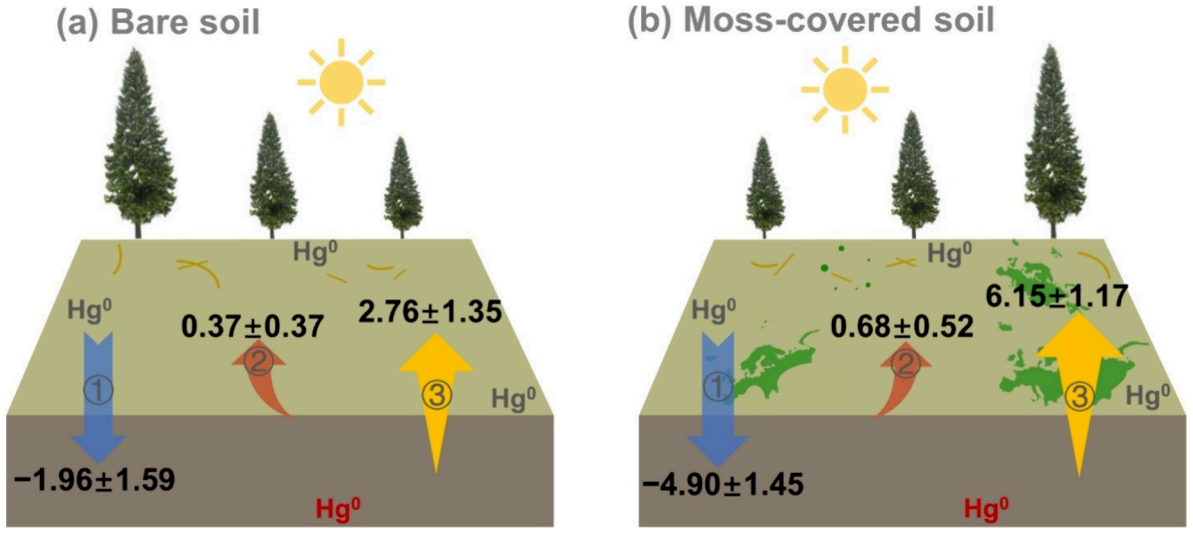

Figure 4. Partitioning of the (net) atmosphere−soil (a. bare soil and b. moss-covered soil) Hg^0 fluxes (ng m^{-2} h^{-1}) in Davos-Seehornwald, Switzerland: ① the atmospheric Hg^0 deposition, ② the Hg^0 re-emission from the soil surface, and ③ Hg^0 re-emission from the deeper soil pool. The Hg^0 exchange rates and its uncertainties were estimated based on the isotopic mass model.[24]

https://doi.org/10.1021/acs.est.3c03576
Environ. Sci. Technol. 2023, 57, 15892−15903

fluxes according to SEM (normalized path coefficient: 0.06) (Figures S2 and S4b,c). Soil pore Hg^0 ($\delta^{202}Hg$: −0.77 ± 0.28‰, $\Delta^{199}Hg$ = −0.43 ± 0.05‰, 1SD, n = 4) has more negative MDF and odd-MIF compared to ambient air ($\delta^{202}Hg$ = 0.54 ± 0.12‰, $\Delta^{199}Hg$ = −0.21 ± 0.02‰, 1SD, n = 6) (Tables S4 and S5). Accordingly, the diffused soil pore Hg^0 was apparently the major cause of the negative shift of $\delta^{202}Hg$ and $\Delta^{199}Hg$ values of the efflux air Hg^0 than the surface ambient air in Davos-Seehornwald (Figure 2). Furthermore, there was no significant correlation between $\delta^{202}Hg$ and $\Delta^{199}Hg$ of the ambient air and the Hg^0 exchange flux, whereas $\delta^{202}Hg$ and $\Delta^{199}Hg$ of the efflux air were both positively correlated with the flux reciprocal ($r > 0.80$, $p < 0.05$, Figure 3c,d). This evidence for re-emitted Hg^0 having $\delta^{202}Hg$ lower than ambient Hg^0 is consistent with a soil Hg source and diffusion through pore gas. Hg isotopic compositions in the efflux air were probably controlled by a binary physical mixing between Hg^0 deposition to soils and Hg^0 re-emission to the atmosphere. Here, we used a linearized binary physical mixing diagram to estimate the mean isotopic signatures of the Hg^0 re-emission endmembers by extrapolating the 1/Flux mean to zero (where efflux air is mostly derived from soil re-emission sources) (Figure 3), which showed $\delta^{202}Hg$ and $\Delta^{199}Hg$ values of approximately 0.08 ± 0.03 and −0.39 ± 0.05‰ (1SD), respectively. Yuan et al.[24] demonstrated that the soil pore Hg^0 exhibited a $\Delta^{199}Hg/\Delta^{201}Hg$ ratio ∼1. Furthermore, the soil pore gas, ambient air, and efflux air in Davos-Seehornwald show a $\Delta^{199}Hg/\Delta^{201}Hg$ ratio of 0.81 ± 0.07 (Figure S7), indicating that Hg^0 re-emission from the soil was mainly constrained by microbial reduction rather than abiotic dark reduction associated with around 1.6.[29]

3.5. Partitioning of the Net Atmosphere−Soil Hg^0 Exchange. Atmosphere−soil Hg^0 exchange occurs bidirectionally, i.e., deposition of atmospheric Hg^0 to the soil by adsorption (① in Figure 4) and re-emission of Hg^0 from the soil to the atmosphere. Re-emission is induced by photoreduction of Hg^{II} on the soil surface (0−1 cm) (② in Figure 4) and microbial as well as abiotic dark reduction in the deeper soil pool (>1 cm) (③ in Figure 4).[82,84,85] Taking advantage of the unique Hg isotope fractionation in each of these processes, Yuan et al.[24] modeled the fluxes of Hg^0 deposition and re-emission at the atmosphere−soil interface of a subtropical forest (Mt. Ailao) in S-China. Specifically, revealing the contribution of photoreduction as well as microbial and abiotic dark reduction to the net Hg^0 re-emission has delivered a new insight into the complexity of the atmosphere−surface exchange of Hg^0 over the forest ecosystem.

In this study, we applied the model developed by Yuan et al.[24] (detailed in Text S1 and Table S6) to partition the Hg^0 exchange at the atmosphere−soil interface in Davos-Seehornwald. The simulated atmospheric Hg^0 deposition flux to the moss-covered soil (−4.90 ± 1.45 ng m^{-2} h^{-1}) was 2.5 times higher compared to that of the bare soil (−1.96 ± 1.59 ng m^{-2} h^{-1}) (Figure 4). Re-emission of Hg^0 from the deeper soil pool (6.15 ± 1.17 and 2.76 ± 1.35 ng m^{-2} h^{-1}, respectively) was 7−9 times higher than that from the surface of moss-covered and bare soil (0.68 ± 0.52 and 0.37 ± 0.37 ng m^{-2} h^{-1}, respectively), reflecting that Hg photoreduction on the surface of the forest soils was largely suppressed due to shading of sunlight by the canopy. Temperature has been shown to predominately control the rate of not only Hg^{II} reduction to Hg^0 by microorganisms but also Hg^0 diffusion in soil pore space.[79,86] This also confirms the key role of the temperature in governing the Hg^0 exchange (Figures S4b,c and S5). The 2.2 times more Hg^0 re-emission through pore gas evasion from moss-covered than bare soils mirrors that the greater Hg^0 re-emission were predominately driven by Hg^{II} microbial and dark abiotic reduction, which is in good agreement with our hypothesis. According to the ratio of moss-covered soil to the whole forest floor area (48%), the normalized fluxes of atmospheric Hg^0 direct deposition to soil, Hg photoreduction, and Hg reduction in the deeper soil pool were estimated to be −3.37 ± 1.52, 0.52 ± 0.44, and 4.39 ± 1.26 ng m^{-2} h^{-1}, respectively.

There are two potential uncertainties encompassed in our modeling here. One is the current lack of knowledge concerning Hg isotope fractionation during particular steps of atmosphere−soil Hg^0 exchange, e.g., adsorption of atmospheric Hg^0 to soil and the subsequent Hg^0 oxidation. Although adsorption of Hg to goethite and thiols have been shown to produce insignificant odd-MIF,[87,88] the applicability of such information to our system is still doubtful due to the much complex matrix in soils. Zhu et al.[25] demonstrated insignificant MIF during atmospheric Hg^0 deposition to soil. Nevertheless, such a conclusion was only based on limited experimental data. A recent study revealed that abiotic dark oxidation by natural humic acids could induce a small positive odd-MIF shift ($E^{199}Hg_{Hg(0)-Hg(II)}$ = −0.18 ± 0.03‰, 1SD) in residual Hg^0.[89] Based on the above analyses, our model assumed that atmospheric Hg^0 deposition to soil would not result in significant odd-MIF. Another uncertainty arisen from the Hg isotopic compositions of different endmembers due to the time constraints of our field study. Even though the model has performed tens of thousands of simulations in the standard deviation range of the endmembers, feeding the endmembers values determined on such data basis could still introduce certain amounts of errors. To significantly improve the model, more comprehensive information about Hg isotope fractionation and isotope signatures during atmosphere−soil exchange processes would be needed in the future.

4. IMPLICATION FOR MERCURY CYCLING IN THE FOREST ECOSYSTEM

Norway spruce needles were a net sink (−1.05 ± 0.33 ng m^{-2} h^{-1}, per ground area) for Hg^0 while the subalpine coniferous forest floor constituted a source (1.53 ± 1.09 ng m^{-2} h^{-1}) of atmospheric Hg^0 in Davos-Seehornwald. Accordingly, the Davos-Seehornwald forest was a weak source (0.48 ± 1.14 ng m^{-2} h^{-1}) of atmospheric Hg^0 during the period of investigation. Surprisingly, the Hg isotope-based modeling highlights atmospheric Hg^0 deposition rate to the forest floor (−3.37 ± 1.52 ng m^{-2} h^{-1}) was about 3 times than the normalized Hg^0 uptake rates (−1.05 ± 0.33 ng m^{-2} h^{-1}) per ground area by needles. Such strong deposition of atmospheric Hg^0 could be attributed to the rapid adsorption and oxidation of deposited Hg^0 in the forest floor due to the high level of reduced sulfur and −N/O functional groups.[89] Therefore, the potential of soil trapping atmospheric Hg^0 needs to be taken more seriously into account when considering terrestrial Hg biogeochemical cycling.

The uptake of atmospheric Hg^0 by needles would deduce Hg^0 concentration in the surrounding atmosphere, which could be partially offset by Hg^0 re-emission from soils. Consequently, the isotope signature of below-canopy atmospheric Hg^0 is a result of the superposition of the two processes, with (1) the ambient atmospheric $\delta^{202}Hg^0$ being more positive

https://doi.org/10.1021/acs.est.3c03576
Environ. Sci. Technol. 2023, 57, 15892−15903

due to needle uptake and (2) the atmospheric $\delta^{202}Hg^0$ being more negative due to soil re-emission. Thus, our research highlights that atmosphere−foliage and atmosphere−soil exchanges not only alter atmospheric Hg^0 concentrations but also jointly influence the Hg^0 isotopic composition.

The atmospheric Hg^0 concentration correlates typically positively with atmosphere−soil Hg^0 exchange at remote sites.[19,71,72] The average atmospheric Hg^0 concentration measured during the atmosphere−soil flux investigations was 0.82 ± 0.16 ng m^{-3} in Davos-Seehornwald, which was much lower than the background concentrations of Hg^0 in the Northern Hemisphere (1.5−1.7 ng m^{-3}).[63] Thus, lower atmospheric Hg^0 concentrations could lead to a higher potential of Hg re-emission from the forest soils in Davos-Seehornwald. Compared to the earlier studies in Europe (−0.9 to 0.8 ng m^{-2} h^{-1}), the current Hg net emission from soils in the Davos-Seehornwald was much higher (1.17−1.93 ng m^{-2} h^{-1}), which could probably result from the declining atmospheric Hg^0 concentrations and rising temperatures. In Europe, the atmospheric Hg^0 concentrations in coniferous forests have been evidenced to decrease from 1.5−6.0 ng m^{-3} in 1987 to 0.39−1.13 ng m^{-3} in 2019 (Table S2). In the Davos-Seehornwald, the mean annual temperature during 2009−2020 increased by +0.4 °C compared to 1997−2008. Based on the formula in Figure S5 and the current annual average air temperature of Davos-Seehornwald (4.5 °C), we have roughly estimated that the average annual atmosphere−soil Hg^0 fluxes would increase from the current 1.07 to 1.41 ng m^{-2} h^{-1} under the target scenario of 2 °C of global warming under the Paris Climate Agreement. In the context of the Minamata Convention aiming to decrease anthropogenic Hg emission and global warming, soils have been regarded as an increasingly important source of atmospheric Hg^0.[12,72]

■ ASSOCIATED CONTENT

Supporting Information

The Supporting Information is available free of charge at https://pubs.acs.org/doi/10.1021/acs.est.3c03576.

Mercury stable isotopic mass balance model (PDF)

■ AUTHOR INFORMATION

Corresponding Authors

Jen-How Huang − *State Key Laboratory of Environmental Geochemistry, Institute of Geochemistry, Chinese Academy of Sciences, Guiyang 550081, China; Environmental Geosciences, University of Basel, 4056 Basel, Switzerland*; Email: jen-howhuang@mail.gyig.ac.cn

Xinbin Feng − *State Key Laboratory of Environmental Geochemistry, Institute of Geochemistry, Chinese Academy of Sciences, Guiyang 550081, China*; orcid.org/0000-0002-7462-8998; Email: fengxinbin@vip.skleg.cn

Authors

Chaoyue Chen − *State Key Laboratory of Environmental Geochemistry, Institute of Geochemistry, Chinese Academy of Sciences, Guiyang 550081, China*

Kai Li − *State Key Laboratory of Environmental Geochemistry, Institute of Geochemistry, Chinese Academy of Sciences, Guiyang 550081, China*

Stefan Osterwalder − *Environmental Geosciences, University of Basel, 4056 Basel, Switzerland; Institute of Agricultural Sciences, ETH Zurich, 8092 Zurich, Switzerland*

Chenmeng Yang − *State Key Laboratory of Environmental Geochemistry, Institute of Geochemistry, Chinese Academy of Sciences, Guiyang 550081, China*

Peter Waldner − *Swiss Federal Institute for Forest, Snow and Landscape Research WSL, 8903 Birmensdorf, Switzerland*

Hui Zhang − *State Key Laboratory of Environmental Geochemistry, Institute of Geochemistry, Chinese Academy of Sciences, Guiyang 550081, China*

Xuewu Fu − *State Key Laboratory of Environmental Geochemistry, Institute of Geochemistry, Chinese Academy of Sciences, Guiyang 550081, China*; orcid.org/0000-0002-5174-7150

Complete contact information is available at: https://pubs.acs.org/10.1021/acs.est.3c03576

Notes

The authors declare no competing financial interest.

■ ACKNOWLEDGMENTS

This study was financially supported by Guizhou Provincial 2019 Science and Technology Subsidies (No. GZ2019SIG), Swiss National Science Foundation IZLCZ2_170176, and the Natural Science Foundation of China (21661132002, 41430754). We thank the Swiss Federal Laboratories for Materials Science and Technology (EMPA), Dr. Christoph Hüglin and Beat Schwarzenbach, and the ETHZ Grassland Sciences group of Prof. Nina Buchmann for providing meteorological data and granting access to the research site. We acknowledge the support from the Swiss Long-term Forest Ecosystem Research Programme LWF and from the Swiss Federal Institute for Forest, Snow and Landscape Research (WSL), in particular, the administrative and logistic support from Jasmin Zimmermann, Markus Jaggi, and Andreas Zurlinden.

■ REFERENCES

(1) UNEP. *Global Mercury Assessment 2018: Technical background report for the global mercury assessment*; UNEP, 2019.

(2) Selin, N. E. Global Biogeochemical Cycling of Mercury: A Review. *Annu. Rev. Environ. Resour.* **2009**, *34*, 43−63.

(3) Gustin, M.; Jaffe, D. Reducing the Uncertainty in Measurement and Understanding of Mercury in the Atmosphere. *Environ. Sci. Technol.* **2010**, *44* (7), 2222−2227.

(4) Schroeder, W. H.; Munthe, J. Atmospheric mercury - An overview. *Atmos. Environ.* **1998**, *32* (5), 809−822.

(5) Horowitz, H. M.; Jacob, D. J.; Zhang, Y. X.; Dibble, T. S.; Slemr, F.; Amos, H. M.; Schmidt, J. A.; Corbitt, E. S.; Marais, E. A.; Sunderland, E. M. A new mechanism for atmospheric mercury redox chemistry: implications for the global mercury budget. *Atmos. Chem. Phys.* **2017**, *17* (10), 6353−6371.

(6) Tsui, M. T. K.; Blum, J. D.; Kwon, S. Y. Review of stable mercury isotopes in ecology and biogeochemistry. *Sci. Total Environ.* **2020**, *716*, No. 135386.

(7) Gustin, M. S.; Bank, M. S.; Bishop, K.; Bowman, K.; Branfireun, B.; Chetelat, J.; Eckley, C. S.; Hammerschmidt, C. R.; Lamborg, C.; Lyman, S.; Martinez-Cortizas, A.; Sommar, J.; Tsui, M. T. K.; Zhang, T. Mercury biogeochemical cycling: A synthesis of recent scientific advances. *Sci. Total Environ.* **2020**, *737*, No. 139619.

(8) Grigal, D. F. Mercury sequestration in forests and peatlands: A review. *J. Environ. Qual.* **2003**, *32* (2), 393−405.

(9) Obrist, D.; Roy, E. M.; Harrison, J. L.; Kwong, C. F.; Munger, J. W.; Moosmuller, H.; Romero, C. D.; Sun, S. W.; Zhou, J.; Commane, R. Previously unaccounted atmospheric mercury deposition in a midlatitude deciduous forest. *Proc. Natl. Acad. Sci. U. S. A.* **2021**, *118* (29), No. e210547711.

(10) Huang, J.-H.; Berg, B.; Chen, C.; Thimonier, A.; Schmitt, M.; Osterwalder, S.; Alewell, C.; Rinklebe, J.; Feng, X. Predominant contributions through lichen and fine litter to litterfall mercury deposition in a subalpine forest. *Environ. Res.* **2023**, *229*, No. 116005.
(11) Zhou, J.; Obrist, D.; Dastoor, A.; Jiskra, M.; Ryjkov, A. Vegetation uptake of mercury and impacts on global cycling. *Nat. Rev. Earth Environ.* **2021**, *2* (4), 269−284.
(12) Yu, Q.; Luo, Y.; Xu, G. Y.; Wu, Q. R.; Wang, S. X.; Hao, J. M.; Duan, L. Subtropical Forests Act as Mercury Sinks but as Net Sources of Gaseous Elemental Mercury in South China. *Environ. Sci. Technol.* **2020**, *54* (5), 2772−2779.
(13) Jiskra, M.; Sonke, J. E.; Obrist, D.; Bieser, J.; Ebinghaus, R.; Myhre, C. L.; Pfaffhuber, K. A.; Wangberg, I.; Kyllonen, K.; Worthy, D.; Martin, L. G.; Labuschagne, C.; Mkololo, T.; Ramonet, M.; Magand, O.; Dommergue, A. A vegetation control on seasonal variations in global atmospheric mercury concentrations. *Nat. Geosci.* **2018**, *11* (4), 244−250.
(14) Fu, X. W.; Zhu, W.; Zhang, H.; Sommar, J.; Yu, B.; Yang, X.; Wang, X.; Lin, C. J.; Feng, X. B. Depletion of atmospheric gaseous elemental mercury by plant uptake at Mt. Changbai, Northeast China. *Atmos. Chem. Phys.* **2016**, *16* (20), 12861−12873.
(15) Wang, X.; Bao, Z. D.; Lin, C. J.; Yuan, W.; Feng, X. B. Assessment of Global Mercury Deposition through Litterfall. *Environ. Sci. Technol.* **2016**, *50* (16), 8548−8557.
(16) Wright, L. P.; Zhang, L. M.; Marsik, F. J. Overview of mercury dry deposition, litterfall, and throughfall studies. *Atmos. Chem. Phys.* **2016**, *16* (21), 13399−13416.
(17) Lindberg, S.; Bullock, R.; Ebinghaus, R.; Engstrom, D.; Feng, X. B.; Fitzgerald, W.; Pirrone, N.; Prestbo, E.; Seigneur, C. A synthesis of progress and uncertainties in attributing the sources of mercury in deposition. *Ambio* **2007**, *36* (1), 19−32.
(18) Bishop, K.; Shanley, J. B.; Riscassi, A.; de Wit, H. A.; Eklof, K.; Meng, B.; Mitchell, C.; Osterwalder, S.; Schuster, P. F.; Webster, J.; Zhu, W. Recent advances in understanding and measurement of mercury in the environment: Terrestrial Hg cycling. *Sci. Total Environ.* **2020**, *721*, No. 137647.
(19) Agnan, Y.; Le Dantec, T.; Moore, C. W.; Edwards, G. C.; Obrist, D. New constraints on terrestrial surface atmosphere fluxes of gaseous elemental mercury using a global database. *Environ. Sci. Technol.* **2016**, *50* (2), 507−524.
(20) Fu, X. W.; Zhang, H.; Liu, C.; Zhang, H.; Lin, C. J.; Feng, X. B. Significant seasonal variations in isotopic composition of atmospheric total gaseous mercury at forest sites in China caused by vegetation and mercury sources. *Environ. Sci. Technol.* **2019**, *53* (23), 13748−13756.
(21) Obrist, D.; Agnan, Y.; Jiskra, M.; Olson, C. L.; Colegrove, D. P.; Hueber, J.; Moore, C. W.; Sonke, J. E.; Helmig, D. Tundra uptake of atmospheric elemental mercury drives Arctic mercury pollution. *Nature* **2017**, *547* (7662), 201−204.
(22) Sun, S. W.; Ma, M.; He, X. B.; Obrist, D.; Zhang, Q. G.; Yin, X. F.; Sun, T.; Huang, J.; Guo, J. M.; Kang, S. C.; Qin, D. H. Vegetation Mediated Mercury Flux and Atmospheric Mercury in the Alpine Permafrost Region of the Central Tibetan Plateau. *Environ. Sci. Technol.* **2020**, *54* (10), 6043−6052.
(23) Obrist, D.; Kirk, J. L.; Zhang, L.; Sunderland, E. M.; Jiskra, M.; Selin, N. E. A review of global environmental mercury processes in response to human and natural perturbations: Changes of emissions, climate, and land use. *Ambio* **2018**, *47* (2), 116−140.
(24) Yuan, W.; Wang, X.; Lin, C. J.; Sommar, J. O.; Wang, B.; Lu, Z. Y.; Feng, X. B. Quantification of Atmospheric Mercury Deposition to and Legacy Re-emission from a Subtropical Forest Floor by Mercury Isotopes. *Environ. Sci. Technol.* **2021**, *55* (18), 12352−12361.
(25) Zhu, W.; Fu, X. W.; Zhang, H.; Liu, C.; Skyllberg, U.; Sommar, J.; Yu, B.; Feng, X. B. Mercury Isotope Fractionation during the Exchange of Hg(0) between the Atmosphere and Land Surfaces: Implications for Hg(0) Exchange Processes and Controls. *Environ. Sci. Technol.* **2022**, *56* (2), 1445−1457.
(26) Sommar, J.; Osterwalder, S.; Zhu, W. Recent advances in understanding and measurement of Hg in the environment: Surface-atmosphere exchange of gaseous elemental mercury (Hg^0). *Sci. Total Environ.* **2020**, *721*, No. 137648.
(27) Blum, J. D.; Sherman, L. S.; Johnson, M. W. Mercury Isotopes in Earth and Environmental Sciences. *Ann. Rev. Earth Planet. Sci.* **2014**, *42*, 249−269.
(28) Bergquist, B. A.; Blum, J. D. Mass-dependent and -independent fractionation of Hg isotopes by photoreduction in aquatic systems. *Science* **2007**, *318* (5849), 417−420.
(29) Zheng, W.; Hintelmann, H. Nuclear Field Shift Effect in Isotope Fractionation of Mercury during Abiotic Reduction in the Absence of Light. *J. Phys. Chem. A* **2010**, *114* (12), 4238−4245.
(30) Wang, X.; Yuan, W.; Lin, C. J.; Feng, X. B. Mercury cycling and isotopic fractionation in global forests. *Crit. Rev. Environ. Sci. Technol.* **2022**, *52* (21), 3763−3786.
(31) Kwon, S. Y.; Blum, J. D.; Yin, R.; Tsui, M. T. K.; Yang, Y. H.; Choi, J. W. Mercury stable isotopes for monitoring the effectiveness of the Minamata Convention on Mercury. *Earth-Sci. Rev.* **2020**, *203*, No. 103111.
(32) Etzold, S.; Ruehr, N. K.; Zweifel, R.; Dobbertin, M.; Zingg, A.; Pluess, P.; Hasler, R.; Eugster, W.; Buchmann, N. The carbon balance of two contrasting mountain forest ecosystems in Switzerland: similar annual trends, but seasonal differences. *Ecosystems* **2011**, *14* (8), 1289−1309.
(33) Chen, C.; Huang, J.-H.; Meusburger, K.; Li, K.; Fu, X.; Rinklebe, J.; Alewell, C.; Feng, X. The interplay between atmospheric deposition and soil dynamics of mercury in Swiss and Chinese boreal forests: A comparison study. *Environ. Pollut.* **2022**, *307*, No. 119483.
(34) Yuan, W.; Sommar, J.; Lin, C. J.; Wang, X.; Li, K.; Liu, Y.; Zhang, H.; Lu, Z. Y.; Wu, C. S.; Feng, X. B. Stable Isotope Evidence Shows Re-emission of Elemental Mercury Vapor Occurring after Reductive Loss from Foliage. *Environ. Sci. Technol.* **2019**, *53* (2), 651−660.
(35) Poissant, L.; Pilote, M.; Yumvihoze, E.; Lean, D. Mercury concentrations and foliage/atmosphere fluxes in a maple forest ecosystem in Quebec, Canada. *J. Geophys. Res. -Atmos.* **2008**, *113* (D10), D10307.
(36) Lin, C. J.; Zhu, W.; Li, X. C.; Feng, X. B.; Sommar, J.; Shang, L. H. Novel Dynamic Flux Chamber for Measuring Air-Surface Exchange of Hg-o from Soils. *Environ. Sci. Technol.* **2012**, *46* (16), 8910−8920.
(37) Yuan, W.; Wang, X.; Lin, C. J.; Sommar, J.; Lu, Z. Y.; Feng, X. B. Process factors driving dynamic exchange of elemental mercury vapor over soil in broadleaf forest ecosystems. *Atmos. Environ.* **2019**, *219*, No. 117047.
(38) Zhu, W.; Sommar, J.; Lin, C. J.; Feng, X. Mercury vapor air-surface exchange measured by collocated micrometeorological and enclosure methods - Part I: Data comparability and method characteristics. *Atmos. Chem. Phys.* **2015**, *15* (2), 685−702.
(39) Sun, R. Y.; Enrico, M.; Heimburger, L. E.; Scott, C.; Sonke, J. E. A double-stage tube furnace-acid-trapping protocol for the pre-concentration of mercury from solid samples for isotopic analysis. *Anal. Bioanal. Chem.* **2013**, *405* (21), 6771−6781.
(40) Fu, X. W.; Heimburger, L. E.; Sonke, J. E. Collection of atmospheric gaseous mercury for stable isotope analysis using iodine- and chlorine-impregnated activated carbon traps. *J. Anal. Atom. Spectrom.* **2014**, *29* (5), 841−852.
(41) USEPA. *Mercury in water by oxidation, purge and trap, and cold vapor atomic fluorescence spectrometry (method 1631, revision E)*. EPA-821-R-02- 019. U.S. EPA: Washington, DC, 2002.
(42) Yin, R. S.; Feng, X. B.; Foucher, D.; Shi, W. F.; Zhao, Z. Q.; Wang, J. High Precision Determination of Mercury Isotope Ratios Using Online Mercury Vapor Generation System Coupled with Multi-collector Inductively Coupled Plasma-Mass Spectrometry. *Chinese J. Anal. Chem.* **2010**, *38* (7), 929−934.
(43) Blum, J. D.; Bergquist, B. A. Reporting of variations in the natural isotopic composition of mercury. *Anal. Bioanal. Chem.* **2007**, *388* (2), 353−359.
(44) Enrico, M.; Le Roux, G.; Marusczak, N.; Heimburger, L. E.; Claustres, A.; Fu, X. W.; Sun, R. Y.; Sonke, J. E. Atmospheric Mercury

Transfer to Peat Bogs Dominated by Gaseous Elemental Mercury Dry Deposition. *Environ. Sci. Technol.* **2016**, *50* (5), 2405−2412.
(45) Wohlgemuth, L.; Osterwalder, S.; Joseph, C.; Kahmen, A.; Hoch, G.; Alewell, C.; Jiskra, M. A bottom-up quantification of foliar mercury uptake fluxes across Europe. *Biogeosciences* **2020**, *17* (24), 6441−6456.
(46) Laacouri, A.; Nater, E. A.; Kolka, R. K. Distribution and uptake dynamics of mercury in leaves of common deciduous tree species in Minnesota, USA. *Environ. Sci. Technol.* **2013**, *47* (18), 10462−10470.
(47) Teixeira, D. C.; Lacerda, L. D.; Silva-Filho, E. V. Foliar mercury content from tropical trees and its correlation with physiological parameters in situ. *Environ. Pollut.* **2018**, *242*, 1050−1057.
(48) Wohlgemuth, L.; Rautio, P.; Ahrends, B.; Russ, A.; Vesterdal, L.; Waldner, P.; Timmermann, V.; Eickenscheidt, N.; Furst, A.; Greve, M.; Roskams, P.; Thimonier, A.; Nicolas, M.; Kowalska, A.; Ingerslev, M.; Merila, P.; Benham, S.; Iacoban, C.; Hoch, G.; Alewell, C.; Jiskra, M. Physiological and climate controls on foliar mercury uptake by European tree species. *Biogeosciences* **2022**, *19* (5), 1335−1353.
(49) Pleijel, H.; Klingberg, J.; Nerentorp, M.; Broberg, M. C.; Nyirambangutse, B.; Munthe, J.; Wallin, G. Mercury accumulation in leaves of different plant types - the significance of tissue age and specific leaf area. *Biogeosciences* **2021**, *18* (23), 6313−6328.
(50) Rutter, A. P.; Schauer, J. J.; Shafer, M. M.; Creswell, J.; Olson, M. R.; Clary, A.; Robinson, M.; Parman, A. M.; Katzman, T. L. Climate Sensitivity of Gaseous Elemental Mercury Dry Deposition to Plants: Impacts of Temperature, Light Intensity, and Plant Species. *Environ. Sci. Technol.* **2011**, *45* (2), 569−575.
(51) Liu, Y. W.; Liu, G. L.; Wang, Z. W.; Guo, Y. Y.; Yin, Y. G.; Zhang, X. S.; Cai, Y.; Jiang, G. B. Understanding foliar accumulation of atmospheric Hg in terrestrial vegetation: Progress and challenges. *Crit. Rev. Environ. Sci. Technol.* **2022**, *52* (24), 4331−4352.
(52) Naharro, R.; Esbri, J. M.; Amoros, J. A.; Higueras, P. L. Experimental assessment of the daily exchange of atmospheric mercury inEpipremnum aureum. *Environ. Geochem. Health* **2020**, *42* (10), 3185−3198.
(53) Osterwalder, S.; Eugster, W.; Feigenwinter, I.; Jiskra, M. Eddy covariance flux measurements of gaseous elemental mercury over a grassland. *Atmos. Meas. Tech.* **2020**, *13* (4), 2057−2074.
(54) Demers, J. D.; Blum, J. D.; Zak, D. R. Mercury isotopes in a forested ecosystem: Implications for air-surface exchange dynamics and the global mercury cycle. *Global Biogeochem. Cycles* **2013**, *27* (1), 222−238.
(55) Kurz, A. Y.; Blum, J. D.; Gratz, L. E.; Jaffe, D. A. Contrasting controls on the diel isotopic variation of Hg^0 at two high elevation sites in the Western United States. *Environ. Sci. Technol.* **2020**, *54* (17), 10502−10513.
(56) Wang, X.; Yuan, W.; Lin, C. J.; Luo, J.; Wang, F. Y.; Feng, X. B.; Fu, X. W.; Liu, C. Underestimated Sink of Atmospheric Mercury in a Deglaciated Forest Chronosequence. *Environ. Sci. Technol.* **2020**, *54* (13), 8083−8093.
(57) Liu, H. W.; Shao, J. J.; Yu, B.; Liang, Y.; Duo, B.; Fu, J. J.; Yang, R. Q.; Shi, J. B.; Jiang, G. B. Mercury isotopic compositions of mosses, conifer needles, and surface soils: Implications for mercury distribution and sources in Shergyla Mountain, Tibetan Plateau. *Ecotoxicol. Environ. Safe* **2019**, *172*, 225−231.
(58) Zheng, W.; Obrist, D.; Weis, D.; Bergquist, B. A. Mercury isotope compositions across North American forests. *Global Biogeochem. Cycles* **2016**, *30* (10), 1475−1492.
(59) Gratz, L. E.; Keeler, G. J.; Blum, J. D.; Sherman, L. S. Isotopic Composition and Fractionation of Mercury in Great Lakes Precipitation and Ambient Air. *Environ. Sci. Technol.* **2010**, *44* (20), 7764−7770.
(60) Wang, X.; Luo, J.; Yuan, W.; Lin, C. J.; Wang, F. Y.; Liu, C.; Wang, G. X.; Feng, X. B. Global warming accelerates uptake of atmospheric mercury in regions experiencing glacier retreat. *Proc. Natl. Acad. Sci. U. S. A.* **2020**, *117* (4), 2049−2055.
(61) Chen, J. B.; Hintelmann, H.; Feng, X. B.; Dimock, B. Unusual fractionation of both odd and even mercury isotopes in precipitation from Peterborough, ON, Canada. *Geochim. Cosmochim. Acta* **2012**, *90*, 33−46.
(62) Fu, X. W.; Liu, C.; Zhang, H.; Xu, Y.; Li, J.; Lyu, X. P.; Zhang, G.; Guo, H.; Wang, X.; Zhang, L. M.; Feng, X. B. Isotopic compositions of atmospheric total gaseous mercury in 10 Chinese cities and implications for land surface emissions. *Atmos. Chem. Phys.* **2021**, *21* (9), 6721−6734.
(63) Sprovieri, F.; Pirrone, N.; Bencardino, M.; D'Amore, F.; Carbone, F.; Cinnirella, S.; Mannarino, V.; Landis, M.; Ebinghaus, R.; Weigelt, A.; Brunke, E. G.; Labuschagne, C.; Martin, L.; Munthe, J.; Wangberg, I.; Artaxo, P.; Morais, F.; Barbosa, H. D. J.; Brito, J.; Cairns, W.; Barbante, C.; Dieguez, M. D.; Garcia, P. E.; Dommergue, A.; Angot, H.; Magand, O.; Skov, H.; Horvat, M.; Kotnik, J.; Read, K. A.; Neves, L. M.; Gawlik, B. M.; Sena, F.; Mashyanov, N.; Obolkin, V.; Wip, D.; Bin Feng, X.; Zhang, H.; Fu, X. W.; Ramachandran, R.; Cossa, D.; Knoery, J.; Marusczak, N.; Nerentorp, M.; Norstrom, C. Atmospheric mercury concentrations observed at ground-based monitoring sites globally distributed in the framework of the GMOS network. *Atmos. Chem. Phys.* **2016**, *16* (18), 11915−11935.
(64) Streets, D. G.; Horowitz, H. M.; Jacob, D.; Lu, Z. F.; Levin, L.; ter Schure, A. F. H.; Sunderland, E. M. Total Mercury Released to the Environment by Human Activities. *Environ. Sci. Technol.* **2017**, *51* (11), 5969−5977.
(65) Wu, Q. R.; Wang, S. X.; Li, G. L.; Liang, S.; Lin, C. J.; Wang, Y. F.; Cai, S. Y.; Liu, K. Y.; Hao, J. M. Temporal Trend and Spatial Distribution of Speciated Atmospheric Mercury Emissions in China During 1978−2014. *Environ. Sci. Technol.* **2016**, *50* (24), 13428−13435.
(66) Dastoor, A.; Wilson, S. J.; Travnikov, O.; Ryjkov, A.; Angot, H.; Christensen, J. H.; Steenhuisen, F.; Muntean, M. Arctic atmospheric mercury: Sources and changes. *Sci. Total Environ.* **2022**, *839*, No. 156213.
(67) Yu, B.; Yang, L.; Liu, H. W.; Xiao, C. L.; Bu, D.; Zhang, Q. Y.; Fu, J. J.; Zhang, Q. G.; Cong, Z. Y.; Liang, Y.; Hu, L. G.; Yin, Y. G.; Shi, J. B.; Jiang, G. B. Tracing the Transboundary Transport of Mercury to the Tibetan Plateau Using Atmospheric Mercury Isotopes. *Environ. Sci. Technol.* **2022**, *56* (3), 1568−1577.
(68) Fu, X. W.; Feng, X. B.; Wang, S. F. Exchange fluxes of Hg between surfaces and atmosphere in the eastern flank of Mount Gongga, Sichuan province, southwestern China. *J. Geophys. Res. -Atmos.* **2008**, *113* (D20), D20306.
(69) Gustin, M. S.; Engle, M.; Ericksen, J.; Lyman, S.; Stamenkovic, J.; Xin, M. Mercury exchange between the atmosphere and low mercury containing substrates. *Appl. Geochem.* **2006**, *21* (11), 1913−1923.
(70) Ci, Z. J.; Peng, F.; Xue, X. A.; Zhang, X. S. Air-surface exchange of gaseous mercury over permafrost soil: an investigation at a high-altitude (4700 m a.s.l.) and remote site in the central Qinghai-Tibet Plateau. *Atmos. Chem. Phys.* **2016**, *16* (22), 14741−14754.
(71) Duan, L.; Sun, X. H.; Luo, Y.; Du, B. Y.; Wang, Q.; Liu, K. Y.; Zhang, J. W.; Wu, Q. R.; Wang, S. X. Soil-atmosphere exchange of gaseous elemental mercury in three subtropical forests with different substrate Hg concentrations. *Atmos. Environ.* **2021**, *244*, No. 117869.
(72) Zhou, J.; Wang, Z. W.; Zhang, X. S.; Driscoll, C. T.; Lin, C. J. Soil-atmosphere exchange flux of total gaseous mercury (TGM) at subtropical and temperate forest catchments. *Atmos. Chem. Phys.* **2020**, *20* (24), 16117−16133.
(73) Graydon, J. A.; St Louis, V. L.; Lindberg, S. E.; Hintelmann, H.; Krabbenhoft, D. P. Investigation of mercury exchange between forest canopy vegetation and the atmosphere using a new dynamic chamber. *Environ. Sci. Technol.* **2006**, *40* (15), 4680−4688.
(74) Luo, Y.; Duan, L.; Driscoll, C. T.; Xu, G. Y.; Shao, M. S.; Taylor, M.; Wang, S. X.; Hao, J. M. Foliage/atmosphere exchange of mercury in a subtropical coniferous forest in south China. *JGR Biogeosci.* **2016**, *121* (7), 2006−2016.
(75) Cannone, N.; Binelli, G.; Worland, M. R.; Convey, P.; Guglielmin, M. CO_2 fluxes among different vegetation types during the growing season in Marguerite Bay (Antarctic Peninsula). *Geoderma* **2012**, *189*, 595−605.

https://doi.org/10.1021/acs.est.3c03576
Environ. Sci. Technol. 2023, 57, 15892−15903

(76) Sun, S. Q.; Liu, T.; Wu, Y. H.; Wang, G. X.; Zhu, B.; DeLuca, T. H.; Wang, Y. Q.; Luo, J. Ground bryophytes regulate net soil carbon efflux: evidence from two subalpine ecosystems on the east edge of the Tibet Plateau. *Plant Soil* **2017**, *417* (1−2), 363−375.
(77) Gustin, M. S.; Stamenkovic, J. Effect of Watering and Soil Moisture on Mercury Emissions from Soils. *Biogeochemistry* **2005**, *76* (2), 215−232.
(78) Xin, M.; Gustin, M. S. Gaseous elemental mercury exchange with low mercury containing soils: Investigation of controlling factors. *Appl. Geochem.* **2007**, *22* (7), 1451−1466.
(79) Pannu, R.; Siciliano, S. D.; O'Driscoll, N. J. Quantifying the effects of soil temperature, moisture and sterilization on elemental mercury formation in boreal soils. *Environ. Pollut.* **2014**, *193*, 138−146.
(80) Kritee, K.; Blum, J. D.; Barkay, T. Mercury Stable Isotope Fractionation during Reduction of Hg(II) by Different Microbial Pathways. *Environ. Sci. Technol.* **2008**, *42* (24), 9171−9177.
(81) Yuan, W.; Wang, X.; Lin, C. J.; Wu, C. S.; Zhang, L. M.; Wang, B.; Sommar, J.; Lu, Z. Y.; Feng, X. B. Stable Mercury Isotope Transition during Postdepositional Decomposition of Biomass in a Forest Ecosystem over Five Centuries. *Environ. Sci. Technol.* **2020**, *54* (14), 8739−8749.
(82) Jiskra, M.; Wiederhold, J. G.; Skyllberg, U.; Kronberg, R. M.; Hajdas, I.; Kretzschmar, R. Mercury Deposition and Re-emission Pathways in Boreal Forest Soils Investigated with Hg Isotope Signatures. *Environ. Sci. Technol.* **2015**, *49* (12), 7188−7196.
(83) Zhou, J.; Wang, Z. W.; Zhang, X. S.; Driscoll, C. T. Measurement of the Vertical Distribution of Gaseous Elemental Mercury Concentration in Soil Pore Air of Subtropical and Temperate Forests. *Environ. Sci. Technol.* **2021**, *55* (3), 2132−2142.
(84) Fritsche, J.; Obrist, D.; Alewell, C. Evidence of microbial control of Hg-0 emissions from uncontaminated terrestrial soils. *J. Plant Nutr. Soil Sci.* **2008**, *171* (2), 200−209.
(85) Carpi, A.; Lindberg, S. E. Sunlight-mediated emission of elemental mercury from soil amended with municipal sewage sludge. *Environ. Sci. Technol.* **1997**, *31* (7), 2085−2091.
(86) Giovanella, P.; Cabral, L.; Bento, F. M.; Gianello, C.; Camargo, F. A. O. Mercury (II) removal by resistant bacterial isolates and mercuric (II) reductase activity in a new strain of Pseudomonas sp B50A. *New Biotechnol.* **2016**, *33* (1), 216−223.
(87) Wiederhold, J. G.; Cramer, C. J.; Daniel, K.; Infante, I.; Bourdon, B.; Kretzschmar, R. Equilibrium Mercury Isotope Fractionation between Dissolved Hg(II) Species and Thiol-Bound Hg. *Environ. Sci. Technol.* **2010**, *44* (11), 4191−4197.
(88) Jiskra, M.; Wiederhold, J. G.; Bourdon, B.; Kretzschmar, R. Solution speciation controls mercury isotope fractionation of Hg (II) sorption to goethite. *Environ. Sci. Technol.* **2012**, *46* (12), 6654−6662.
(89) Zheng, W.; Demers, J. D.; Lu, X.; Bergquist, B. A.; Anbar, A. D.; Blum, J. D.; Gu, B. H. Mercury Stable Isotope Fractionation during Abiotic Dark Oxidation in the Presence of Thiols and Natural Organic Matter. *Environ. Sci. Technol.* **2019**, *53* (4), 1853−1862.
(90) Demers, J. D.; Sherman, L. S.; Blum, J. D.; Marsik, F. J.; Dvonch, J. T. Coupling atmospheric mercury isotope ratios and meteorology to identify sources of mercury impacting a coastal urban-industrial region near Pensacola, Florida, USA. *Global Biogeochem. Cycles* **2015**, *29* (10), 1689−1705.

https://doi.org/10.1021/acs.est.3c03576
Environ. Sci. Technol. 2023, 57, 15892−15903